

Probing black hole charge with gravitational microlensing of gravitational waves

Uddeepa Deka,^{1,*} Sumanta Chakraborty,^{2,†} Shasvath J. Kapadia,^{3,1,‡} Md Arif Shaikh,^{4,1,§} and Parameswaran Ajith^{1,¶}

¹International Centre for Theoretical Sciences, Tata Institute of Fundamental Research, Bangalore 560089, India

²Indian Association for the Cultivation of Science, 2A & 2B Raja S C Mullick Road, Kolkata 700032, India

³The Inter-University Centre for Astronomy and Astrophysics, Post Bag 4, Ganeshkhind, Pune 411007, India

⁴Department of Physics and Astronomy, Seoul National University, Seoul 08826, Korea

(Dated: January 15, 2024)

Gravitational microlensing of gravitational waves (GWs) opens up the exciting possibility of studying the spacetime geometry around the lens. In this work, we investigate the prospects of constraining the ‘charged’ hair of a black hole (BH) from the observation of a GW signal microlensed by the BH. The charge can have electromagnetic or modified gravity origin. We compute the analytic form of the lensing potential with charge and construct the lensed waveforms for a range of BH mass, charge and impact parameters, assuming non-spinning BHs. Using an approximate likelihood function, we explore how future observations of microlensed GWs can constrain the charge of the BH lens. We find that positive values of the charge parameter (that can be of electromagnetic or modified gravity origin) can be tightly constrained using lensed GW signals, while the constraints on negative values of the charge parameter (modified gravity origin) are modest.

I. INTRODUCTION

The LIGO and Virgo gravitational-wave (GW) detectors have observed ~ 90 compact binary coalescence (CBC) events during its first three observing runs (O1, O2, O3) [1]. Most of them are binary black hole (BBH) mergers. The remaining are mergers of binary neutron stars (BNSs) [2, 3] and neutron star-black hole (NSBH) binaries [4].

These detections have enabled some of the most unique and stringent tests of general relativity (GR) in the strong-field regime [5]. These include a model-agnostic residual test that studies the statistical properties of the strain data after subtracting out the expected GW signal buried therein to ascertain if the residual is consistent with noise [6–8]; an inspiral-merger-ringdown consistency test that checks if the GW waveform is consistent with GR’s prediction of the same by comparing the binary’s intrinsic parameters inferred from the low- and high-frequency portions of the waveform [9, 10]; a test that compares the speed of GWs with respect to the speed of light [11], as well as one that probes signatures of velocity dispersion as a consequence of a finite graviton mass [12]; and a test of GW polarizations that searches for polarizations of GWs beyond the two predicted by GR [13–16].

The anticipated observations of gravitationally lensed GWs in future observing runs¹ promise to enable additional novel tests of GR (see, e.g., [26–34]), while also shedding light on a number of questions in astrophysics (see, e.g., [35–37]) and cosmology (see, e.g., [38–40]). As with electromagnetic (EM) waves, lensing of GWs results when large agglomerations of

matter lead to deviations in the trajectories of these waves [41–45].

Unlike the case involving EM waves, GW lensing is typically studied in two different regimes. Lensing by galaxies or clusters can be analyzed using the geometric optics (ray-optics) approximation since the wavelengths of the GWs (detectable by LIGO-Virgo) are much smaller than the gravitational radii of such lenses [46–48]. Strong lensing in this regime results in the production of multiple copies of the GWs [49, 50] separated by time delays spanning minutes to months [37, 51, 52]. On the other hand, lensing of GWs by massive compact objects with gravitational radii comparable to the GW wavelength will incur wave optics effects [38, 53–56]. The result is the production of a single image with a modulated GW shape [44]. This shape carries with it imprints of the properties of the lens, and can possibly be used to probe the nature of the compact lens.

Wave-optics effects modulating the GW waveform have been studied extensively for simple lensing potential models, in particular the one corresponding to the point mass lens² [44, 53, 57]. In this model, the frequency-dependent amplitude modulations of the GW waveform are exclusively determined by the (redshifted) mass of the lens, and the impact parameter (i.e., the location of the source in the lens plane) [53]. However, if the compact object has additional hairs, they are also going to show up in the lensed GW waveform, and can possibly be detected as and when microlensed GW signals are observed. The additional hairs could point to the specific nature of the compact object or point to a deviation from GR.

Besides the mass, the next obvious hair that a static and spherically symmetric compact object can have is the electric charge q , which modifies the radial and temporal components of the spacetime metric by $O(Q/r^2)$, where $Q \equiv q^2$. Indeed, it is widely believed that astrophysical objects should not have any net electric charge, or, even if there is some electric charge, it should immediately get shielded [58–60] or neutralised [61].

* uddeepa.deka@icts.res.in

† tpsc@iacs.res.in

‡ shasvath.kapadia@iucaa.in

§ arifshaikh.astro@gmail.com

¶ ajith@icts.res.in

¹ No confirmed detection of GW lensing have thus far been reported [17–23]. Some arguments claiming the observation of lensed GWs – based on the larger BH masses uncovered by GW observations relative to those inferred from galactic X-ray binaries – have been made [24, 25].

² Indeed, most searches for microlensing signatures incurred by wave-optics effects in detected GW events assume a point-mass lens model [17, 21, 38].

Intriguingly, such a ‘charge-like’ hair can arise from several other contexts as well and can have non-negligible values. For example, in the context of an extra spatial dimension, where we live in a four dimensional universe embedded in a five dimensional spacetime, known as the braneworld scenario, the solution of the effective gravitational field equations on the four-dimensional brane has exactly the same structure, but with Q being *negative* [62–66]. Similarly, a positive value of Q can arise in scalar coupled Maxwell theories, described by Horndeski theories [67–69]. There have already been extensive searches for both positive as well as negative values of the ‘charge’ in various contexts — (a) in the weak field regime, e.g., through solar system tests [70–74], (b) using EM waves from accretion on supermassive BHs [75–78], (c) using GWs from BBH and BNS coalescence [79–88], and (d) with strong lensing of EM waves and measurement of BH shadow [89–92].

Here we explore the possibility of constraining the charge hair of a BH from the observation of GWs microlensed by it. We study the lensing-induced modulations on the GW signal by introducing the charge in the lensing potential. In particular, we model the spacetime surrounding the lens to be described by a metric that is analogous to the Reisner-Nordström spacetime, but with $\pm(Q/r^2)$ term in the temporal and radial metric elements. If a lensed GW signal suggest a positive value of Q , it is to be interpreted either in the context of EM-charged BH, or, as a BH in modified theories of gravity. While, if the lensed GW signal prefers a negative value for Q , then it will provide a hint for the existence of extra dimensions. In what follows we will evaluate the lensing potential associated with the new metric, and numerically calculate the corresponding frequency-dependent magnification function that modulates the GW, for a range of the lens masses, impact parameters (i.e., the angular location of the source in the image plane), and the charge Q .

To assess our ability to constrain the charge Q , we quantify the extent to which the GW signal lensed by a BH of charge Q deviates from another waveform lensed by a BH of charge Q_{true} . To that end, we compute matches, defined as the inner product between two waveforms weighted by the noise power spectral density (PSD) of the GW detector. We then use these to construct an approximate likelihood on the lens parameters, which we sample to assess how well we can recover the true value of the charge. We find that positive charges can be well constrained, where a lens with a charge of $Q = 0.1$ can be identified as a charged lens at $> 90\%$ confidence. On the other hand, negatively charged lenses are weakly constrainable – only large $|Q|$ ’s can be constrained well enough to exclude $Q = 0$ at $> 90\%$ confidence.

The paper is organized as follows: In Section II, we present the analytical expression for the lensing potential in the presence of the charge Q . Using the expression for the lensing potential, in Section III we numerically compute the magnification function, as well as the GW waveform lensed by a charged BH. In Section IV we explore the possibility of constraining the charge parameter of a BH from the observation of GWs microlensed by it. We conclude in Section V. Some of the detailed calculations are presented in Appendix A.

Notations and Conventions: We will set the fundamental

constants G and c to unity and will use the mostly positive signature convention, such that the Minkowski metric in Cartesian coordinate takes the form $\eta_{\mu\nu} = \text{diag}(-1, +1, +1, +1)$. Greek indices μ, ν, \dots denote four-dimensional spacetime coordinates, while uppercase Roman indices A, B, \dots denote five-dimensional spacetime indices.

We will refer to Q as the ‘charge’, or ‘charge hair’ of a BH. Note that, even a negative electric charge q will correspond to a positive value of Q , since $Q \equiv q^2$. Also, we will refer to lensing in the wave optics regime ($GM_L/c^2 \sim \lambda_{\text{GW}}$) as microlensing.

II. LENSING MAGNIFICATION BY A CHARGED BLACK HOLE

In this section, we will determine the magnification function due to the simplest possible hair of a BH, namely a charge that can either have an EM origin or, may arise from theories of gravity beyond GR. Of course, any EM charge is expected to be dissipated away with time, or, would be heavily shielded by surrounding matter. But it would still be interesting [58–60] if any residual electric charge present in an astrophysical BH, whether it could be tested using gravitational lensing. More interesting is the case when this charge arises from an alternative theory of gravity. We will provide some examples of such modified theories below.

First of all, the presence of an extra spatial dimension can induce such a charge in the four-dimensional spacetime metric outside of a BH. This is because the effective gravitational field equations on the four-dimensional vacuum spacetime (known as the brane) take the following form [62, 63]

$$G_{\mu\nu} + E_{\mu\nu} = 0. \quad (1)$$

Here $G_{\mu\nu}$ is the four-dimensional Einstein tensor and $E_{\mu\nu} = W_{ABCD}e_\mu^A n^B e_\nu^C n^D$ is the projected five dimensional Weyl tensor on the brane, with e_μ^A being the projector and n_A being the normal to the brane. Owing to the symmetries of the Weyl tensor, it follows that $E_\mu^\mu = 0$, which is akin to the traceless property of the energy-momentum tensor of the EM field. Thus the above field equation for the metric admits the following static and spherically symmetric solution, $-g_{tt} = g^{rr} = 1 - (2M/r) + (Q/r^2)$, with $Q < 0$ and thus differing from the Reissner-Nordström solution by the sign of the $(1/r^2)$ term. In the $f(R)$ gravity as well the same solution for the metric components was obtained [71], however, with a positive contribution from the charge term Q . The Einstein-Gauss-Bonnet theory in higher dimension also admits the same solution on the brane with $Q < 0$, albeit the origin of the charge term was from the coupling constant in the Gauss-Bonnet invariant [66]. Finally, the same solution also arises in the context of a sub-class of Horndeski theories of gravity, which involves the following terms: $\beta G^{\mu\nu} \partial_\mu \phi \partial_\nu \phi$, as well as $-(\gamma/2) T^{\mu\nu} \partial_\mu \phi \partial_\nu \phi$ in the gravitational action, besides the Ricci scalar and the Maxwell term. In this case, the charge Q depends on the ratio (γ/β) and is a positive quantity [67]. Thus, we observe that various cases yield the same metric, with different origin and sign for the charge term. In summary, there are several possibilities for a positive charge to appear in

the metric — (a) EM charge, (b) charge arising from the $f(T)$ theory of gravity, (c) charge depending on the non-trivial coupling between gravity and electromagnetism with scalar, as in Horndeski theories. While the negative charge predominantly arises in the presence of higher dimensions, either from the bulk Weyl tensor or, from the Gauss-Bonnet coupling. This makes the charged metric an ideal ground to probe, since it arises in so many different contexts, with many varieties and hence it is worthwhile to see the effect of such a charge on the microlensing of GWs. In particular, when the wavelength of GWs are comparable to the radius of the event horizon of these charged BHs wave effects must be taken into account. In what follows, we compute the effect of this charge term on the amplification of GWs due to microlensing.

We will work within the thin lens approximation, i.e., the lens is not considered a three-dimensional object, but rather a two-dimensional one. This is because the size of the lens is much smaller compared to the distance of the lens to the source as well as to the observer. Thus the magnification function of the GW, as measured by an observer reads [53],

$$\mathcal{F}(f) = \frac{D_S \xi_0^2}{D_L D_{LS}} \frac{f}{i} \int d^2 \vec{x} \exp[2\pi i f t_d(\vec{x}, \vec{y})], \quad (2)$$

where $\vec{x} \equiv \vec{\xi}/\xi_0$ is the normalized vector on the lens plane and $\vec{y} = (D_L/\xi_0 D_S) \vec{\eta}$ is the normalized vector on the source plane indicating the location of the source (impact parameter). Further, D_L is the angular diameter distance to the lens, D_S is the angular diameter distance to the source and D_{LS} is the angular diameter distance between the source and the lens. Further, the quantity t_d is the time taken by the GW to reach the observer from the source when a lens is present, while f is the frequency of the GW emitted from the source. Since the source and the observer, in general, are separated by a cosmological distance, the effect of the cosmological expansion must be included in the above analysis. This modifies the above magnification function to,

$$\mathcal{F}(f) = \frac{D_S \xi_0^2 (1 + z_L)}{D_L D_{LS}} \frac{f}{i} \int d^2 \vec{x} \exp[2\pi i f t_d(\vec{x}, \vec{y})], \quad (3)$$

where, z_L is the redshift of the lens. Note that the magnification function $\mathcal{F}(f)$ is so chosen that $|\mathcal{F}(f)| = 1$ in the absence of the lens. The time taken by the GW to arrive at the observer from the lens is given by,

$$t_d(\vec{x}, \vec{y}) = \frac{D_S \xi_0^2 (1 + z_L)}{D_L D_{LS}} \left[\frac{|\vec{x} - \vec{y}|^2}{2} - \psi(\vec{x}) \right]. \quad (4)$$

Here $\psi(\vec{x})$ is the two-dimensional deflection potential, depending on the background geometry of the lens, on which the GW is propagating and it satisfies the following differential equation,

$$\nabla_x^2 \psi = \frac{2\Sigma}{\Sigma_{cr}}, \quad (5)$$

where, Σ is the surface energy density of the lens on the lens plane and Σ_{cr} is a critical energy density, to be fixed later. For a

point mass lens, one can simply consider, $\Sigma = M_L \delta^2(\vec{\xi})$, i.e., we can take the point mass to be at the origin of the lens plane. In this case, choosing $\Sigma_{cr} = (M_L/\pi \xi_0^2)$, one obtains, $\psi(\vec{x}) = \ln |\vec{x}|$. In the present context, we are interested in a charged lens, which is either sourced by an EM field or, arises in gravity theories beyond GR. The effects of these modified theories of gravity are embedded through additional contributions to the Einstein's equations and effectively behave as a 'charged' field. In each of these cases, the energy density arising from the extra contribution is given by, $\rho_Q = (Q/r^4)$, or, the associated field behaves as $O(r^{-2})$ in three space dimensions [93]. Thus on the lens plane, which is a two-dimensional hypersurface, the falloff of the field will simply become $O(r^{-1})$ and hence the energy density becomes $(Q/|\vec{\xi}|^2)$ [94–97]. Thus the total energy density on the two-dimensional surface becomes,

$$\Sigma = M_L \delta^2(\vec{\xi}) + \frac{Q}{|\vec{\xi}|^2}. \quad (6)$$

Given the above surface energy density, which involves both the contribution from the point-mass lens and from the charge Q , the two-dimensional gravitational potential can be obtained by solving Eq. (5), and that yields (see Appendix A),

$$\psi(\vec{x}) = \ln |\vec{x}| \left(1 + \frac{\pi Q}{M_L} \ln |\vec{x}| \right). \quad (7)$$

Here, we have chosen the critical surface energy density Σ_{cr} , such that in the limit $Q \rightarrow 0$, we obtain an identical expression to that of the point mass lens. This is one of the main results of this paper.

Given this gravitational potential, in the geometric optics regime, the location of the images on the lens plane can be determined by invoking Fermat's principle of gravitational lensing [98]. Fermat's principle states that the images are formed at the extrema of the time delay surface, that is, at points on the lens plane satisfying the condition:

$$\frac{\partial t_d(\vec{x}, \vec{y})}{\partial \vec{x}} = 0. \quad (8)$$

Thus, the image locations can be obtained by solving the following algebraic equation

$$\frac{D_S \xi_0^2}{D_L D_{LS}} (1 + z_L) \left[|\vec{x} - \vec{y}| - \frac{1}{|\vec{x}|} \left(1 + \frac{2\pi Q}{M_L} \ln |\vec{x}| \right) \right] \frac{\vec{x}}{|\vec{x}|} = 0. \quad (9)$$

Note that GW microlensing happens in the wave optics regime, where the geometric approximation is not valid. However, an approximate understanding of the image locations are useful in interpreting the lensing magnification that we compute in the wave optics regime.

It turns out that for $Q \leq 0$, the above algebraic equation has two solutions for \vec{x} , the normalized vector on the lens plane. These will be the image locations in the geometric optics limit. One of these solutions corresponds to the saddle point, while the other is the minima, as depicted in the left and centre panels in Fig. 1. Besides the locations of these two points, Fig. 1 shows the contours of constant $t_d(\vec{x}, \vec{y})$ for a fixed source location \vec{y} . Interestingly, for certain choices of $Q > 0$, and the

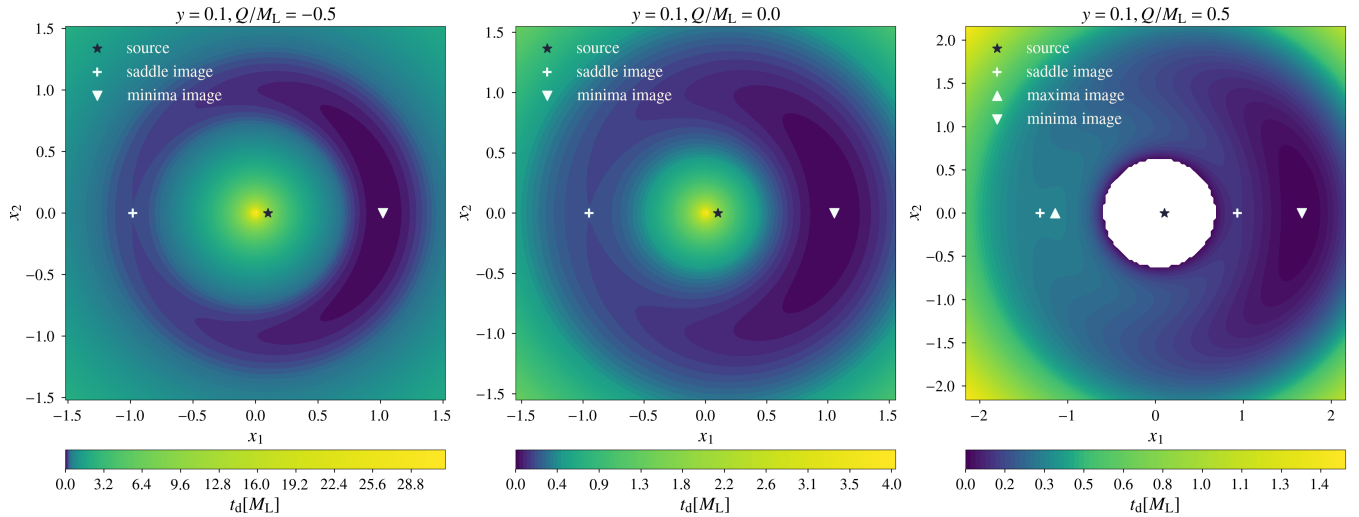


Figure 1. The time delay contours (in units of M_L , where $t_d = 0$ at the global minima) as a function of the lens plane coordinates (x_1, x_2) . The source position is shown by a star ($y = 0.1$). The left, center, and right panels correspond to the cases with $Q/M_L = -0.5, 0$ and 0.5 , respectively. For each of these cases, the locations of the images and their types are also indicated.

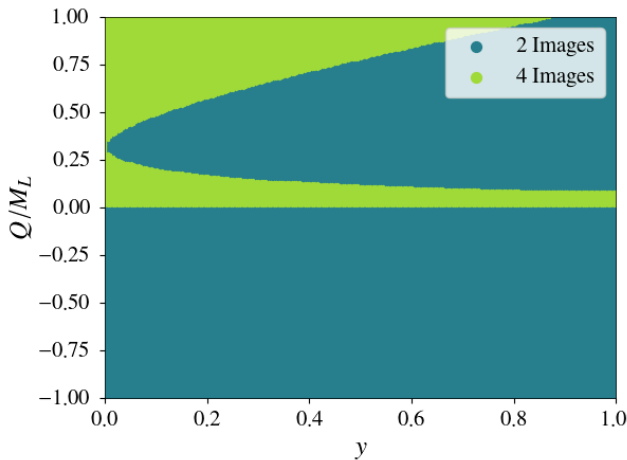


Figure 2. Number of images shown as a function of the impact parameter $|\vec{b}|$, and the charge Q/M_L . There exist two images for all $Q/M_L \leq 0$, irrespective of the impact parameter. However, for $Q/M_L > 0$, there exists a region in the parameter space in which four images are formed. See text for discussion.

impact parameter $|\vec{b}|$, there can even be four solutions to Eq. (9) for \vec{x} , leading to the formation of four images. This can be seen in Fig. 2 and the right panel in Fig. 1.

The formation of multiple images can be understood using caustics associated with the lensing potential. For $Q \leq 0$, there are no caustics (except for the lens location) and hence there are always two images. For any $Q > 0$, a caustic appears at a finite value of $|\vec{b}|$, which decreases as the charge increases. Therefore, for $Q \lesssim 0.1$, the source will appear within the caustic, leading to four images. As the charge increases, the caustic appears at smaller values of $|\vec{b}|$, and for $Q \sim 0.3$, the caustic reaches $|\vec{b}| \sim 0$. Thus the source goes out of the caustic,

leading to two images. Subsequent increase of Q , results in the caustic forming at a larger value of $|\vec{b}|$, and hence the source again goes within the caustic, leading to four images. This is precisely what Fig. 2 demonstrates.

Note that the above situation cannot be compared with the scenario involving the BH shadow, which involves the lensing of EM waves in the strong gravity regime. There, the source (emission from the accreting gas) is close to the lens and the light rays experience the full three-dimensional potential of the lens. In contrast, typical gravitational lensing (as considered here) considers the weak field regime. Also, the distance between the source and the lens is so large that the lens can be approximated by a projected two-dimensional potential (thin lens approximation). Hence the details of the images are quantitatively different in the two scenarios.

Another interesting feature of Fig. 1 corresponds to the fact that images and the source appear along a line in the plane spanned by \vec{x} , which arises from the axially symmetric nature of the lens. This is also reflected in the fact that the lensing potential $\psi(\vec{x})$ depends on $|\vec{x}|$ alone. Thus it follows that the solution of Eq. (9) depends on $|\vec{b}|$ alone, and hence throughout the rest of the analysis we will denote $y \equiv |\vec{b}|$, which is the only input required for determining the image location and the associated time delay contours.

III. NUMERICAL COMPUTATION OF THE LENSING MAGNIFICATION

In this section, we will determine the magnification function due to a charged lens and will find out how the GW waveform is modulated due to lensing. For an isolated point mass lens, the lensing magnification function $\mathcal{F}(f)$ can be derived analytically [57]. Unfortunately, for the present case of a charged lens, an analytical expression for the magnification function

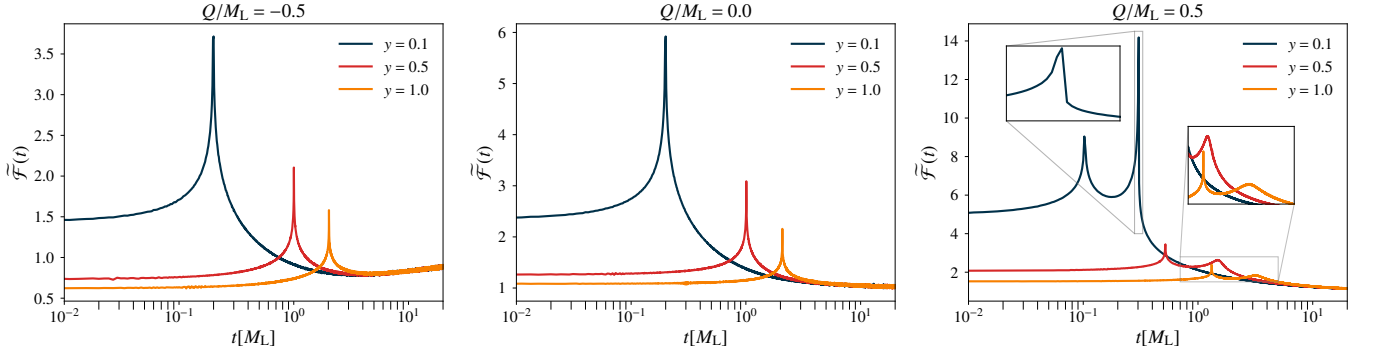


Figure 3. The time domain magnification function $\tilde{\mathcal{F}}(t)$ as a function of time t (in units of M_L , where $t = 0$ at the global minima). The panels from left to right correspond to cases with $Q/M_L = -0.5, 0$ and 0.5 , respectively. The plots in each of these panels correspond to impact parameter values $y = 0.1, 0.5$ and 1.0 . In the left and the center panels, there are always two images – a minima image and a saddle image. The minima image lies at $t = 0$ while the saddle image can be identified by the logarithmically diverging peak. On the right panel, for $y = 0.1$, there are four images – one minima image, two saddle images, and one maxima image. The maxima image and one of the saddle images have similar time delays, $t \sim 0.3$. These two images can be identified by the logarithmic divergence followed by a sharp drop in the zoomed-inset figure on the left. For $y = 0.5$ and 1.0 , there is a minima and a saddle image. However, there are features in addition to the images as seen in the inset figure on the right.

cannot be obtained and one must resort to numerical schemes. Implementing such numerical schemes is also difficult in the present context owing to the highly oscillatory behaviour of the integral, which renders the traditional numerical integration methods to be computationally ineffective. Therefore, we developed and implemented a new numerical scheme to compute the magnification function, which we outline below. This is an extension of the methods used in [55], based on the original work by [99]. The new ingredient is to use a histogram for an efficient computation of the diffraction integral Eq.(13) in time domain.

1. **FIXING THE LENGTH SCALE ξ_0 :** The time delay contours, as well as the lensing potential, depend on the length scale ξ_0 , which we fix to be of the following form:

$$\xi_0^2 = 4M_0 \frac{D_L D_{LS}}{D_S}, \quad (10)$$

where M_0 is an arbitrary mass scale. In the present problem, the only relevant mass scale is set by the lens mass and hence we choose $M_0 = M_L$. With this choice of the length scale ξ_0 , Eq. (4) becomes,

$$t_d(\vec{x}, \vec{y}) = 4M_L(1 + z_L) \times \left[\frac{|\vec{x} - \vec{y}|^2}{2} - \psi(\vec{x}) \right]. \quad (11)$$

In the subsequent analysis, we will use the above expression for the time delay.

2. **TIME DOMAIN MAGNIFICATION FUNCTION:** As we have already discussed, determining the magnification function $\mathcal{F}(f)$ in the frequency domain requires performing the highly oscillatory integral over the time function $t_d(\vec{x}, \vec{y})$, which is numerically challenging. Thus, we will first compute the magnification function in time domain, and then compute $\mathcal{F}(f)$ using Fourier transform. For this purpose

we rewrite Eq. (3) in the following form:

$$\mathcal{F}(f) = C(f) \int d^2\vec{x} \exp[2\pi i f t_d(\vec{x}, \vec{y})]. \quad (12)$$

We define the time domain magnification function $\tilde{\mathcal{F}}(t)$ as the inverse Fourier transform of the ratio $\{\mathcal{F}(f)/C(f)\}$, which yields:

$$\begin{aligned} \tilde{\mathcal{F}}(t) &\equiv \int df \frac{\mathcal{F}(f)}{C(f)} \exp[-2\pi i f t] \\ &= \int d^2\vec{x} \delta[t_d(\vec{x}, \vec{y}) - t]. \end{aligned} \quad (13)$$

As evident from the above expression, the time-domain magnification function is related to the area between the time-domain contours in the lens plane. In particular, $\tilde{\mathcal{F}}(t)dt$ is the area dS between the curves t and $t + dt$ of constant time delay, i.e.,

$$\tilde{\mathcal{F}}(t) = \frac{dS}{dt}. \quad (14)$$

Thus by computing the area between two infinitesimal time domain contours, we can determine the magnification function $\tilde{\mathcal{F}}(t)$ in the time domain.

3. **HISTOGRAM OF THE TIME DELAY MAP:** To find the area between the contours of constant time delay, we place a uniform grid on the lens plane and determine the time delay at each of the grid points (see, e.g., Fig. 1). This yields the number of grid points between time delays t and $t + dt$, which leads to a histogram for the number of grid points at each of the time delay contours t , with bin size dt . This number is a proxy for the area between the time delays t and $t + dt$. Thereby allowing us to compute the time-domain magnification function $\tilde{\mathcal{F}}(t)$.

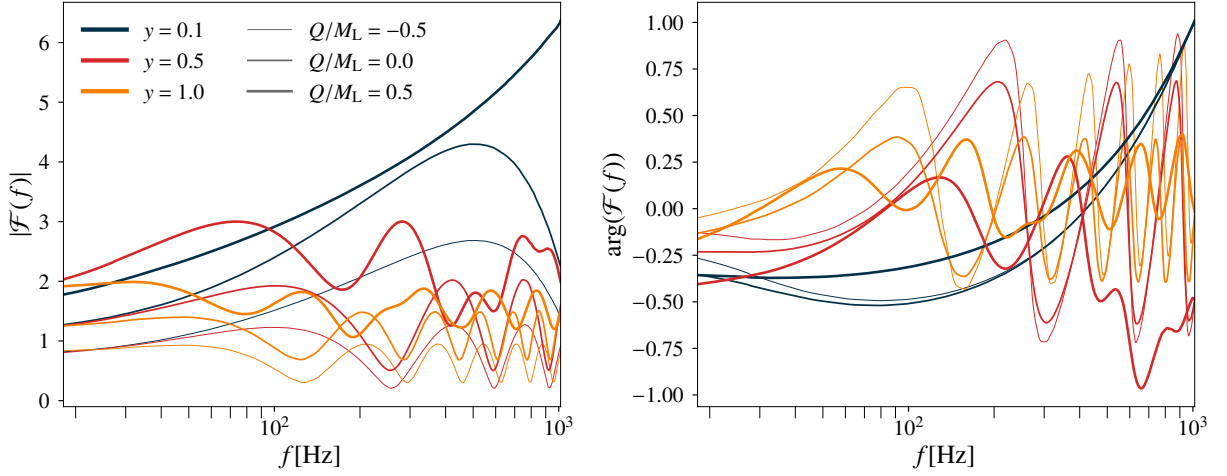


Figure 4. The frequency domain magnification function $\mathcal{F}(f)$ as a function of the GW frequency (in Hz) for a lens with mass $M_L = 100M_\odot$, at redshift $z_L = 0.5$. The left panel corresponds to the amplitude of $\mathcal{F}(f)$, while the right panel corresponds to its phase. The plots corresponds to cases with $Q/M_L = -0.5, 0$ and 0.5 (lines with different thicknesses), for impact parameter values $y = 0.1, 0.5$ and 1.0 (lines with different colors). We restrict the frequencies to the sensitivity band of the ground-based GW detectors.

For the case of a charged lens, the above method of determining the area between time delay contours leads to the desired time-domain magnification function (Fig. 3). As evident, the amplification is lowest for $Q < 0$ and is the highest for $Q > 0$. Also, the magnification function increases as the impact parameter y is decreased, since the GW passes closer to the lens and is most affected. Another intriguing feature, already noted earlier, can also be seen in Fig. 3, namely, the existence of four images for certain positive values of Q and for specific impact parameter y . For $Q/M_L = 0.5$ and $y = 0.1$, these four images can be seen explicitly. The one at $t = 0$ is present in all the plots, which have not been shown, then two additional images are clearly visible, while the fourth one (maxima image) is very close to one of the saddle images. For larger values of y , there are two images with positive Q , but some additional features are present. These can be seen in the inset figures of the right panel in Fig. 3.

4. **FREQUENCY DOMAIN MAGNIFICATION FUNCTION:** Having computed the time-domain magnification function $\tilde{\mathcal{F}}(t)$, it is straightforward to determine the frequency domain magnification $\mathcal{F}(f)$. For this purpose, we simply perform a fast Fourier Transform of $\tilde{\mathcal{F}}(t)$ and multiply by the overall factor $C(f)$, yielding:

$$\mathcal{F}(f) = C(f) \times \text{FFT}[\tilde{\mathcal{F}}(t)] . \quad (15)$$

Though the time-domain magnification function was real, the frequency-domain amplification is complex. Following this, we have plotted the magnitude $|\mathcal{F}(f)|$ and the argument $\arg[\mathcal{F}(f)]$ in Fig. 4. As expected, the frequency-domain magnification also is the largest for $Q > 0$, while is the smallest for $Q < 0$, and the magnification function decreases as the impact parameter increases.

5. **LENSED WAVEFORM:** Finally, the GW strain is going to be amplified by the frequency-dependent magnification factor. In the frequency domain, the unlensed GW strain $h^U(f|\vec{\theta})$ is going to be modified as:

$$h^L(f; \vec{\theta}, \vec{\lambda}) = \mathcal{F}(f; \vec{\lambda}) h^U(f; \vec{\theta}) . \quad (16)$$

Here $h^L(f; \vec{\theta}, \vec{\lambda})$ is the lensed waveform, $\vec{\theta}$ are the source parameters of the GW signal and $\vec{\lambda} = (M_L^z, y, Q)$ are the lens parameters, where $M_L^z \equiv M_L(1+z_L)$ is the redshifted lens mass.

The GW signal lensed by a charged lens has been shown in both the frequency and the time domain in Fig. 5, along with the corresponding unlensed waveform. It is evident (in particular, from the time domain plots) that the lensed waveform for $Q < 0$ has the least departure, while for $Q > 0$ has the maximum departure from the unlensed waveform. For $Q < 0$, the lensed and unlensed waveforms are mostly in phase with the unlensed, while for $Q > 0$, these waveforms are out of phase. As we will see, these properties make constraining positive Q much easier, than constraining negative values of Q .

As a verification of the numerical scheme described above, we have employed the above method for determining the lensed waveform for a point mass (uncharged) lens. Since the magnification function for a point mass lens can be computed analytically [44], we can compare it with our numerical results. Following this, we have evaluated the mismatch between the lensed waveforms computed using the analytical form of the magnification function for isolated point mass lens and lensed waveforms computed using our method with $Q = 0$. We find that the mismatch values are within permissible limits ($\lesssim 10^{-5}$). This validates the numerical method described above and has been used for determining the magnification function for a charged lens.

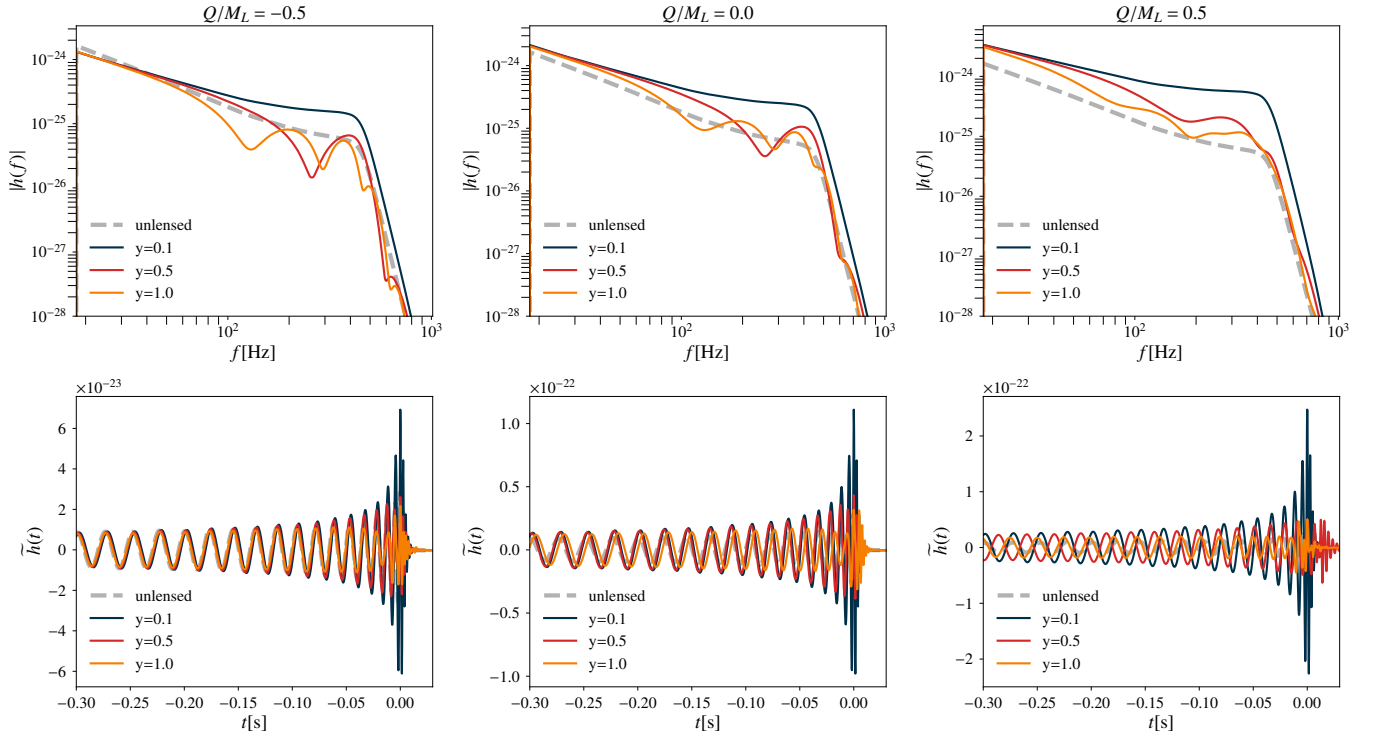


Figure 5. GW signals lensed by charged BHs of mass $M_L = 100M_\odot$, at redshift $z_L = 0.5$. The panels from the left to the right correspond to cases with $Q/M_L = -0.5, 0$ and 0.5 respectively, for various impact parameters (shown in legends). The top and bottom panels show the amplitude of lensed waveforms in the frequency and time domains, respectively. The dashed grey lines indicate the unlensed waveforms.

IV. PROSPECTIVE CONSTRAINTS ON THE BLACK HOLE CHARGE FROM LENSING OBSERVATIONS

In this section, we will derive prospective constraints on the BH charge from future observations of microlensed GW signals. We have already noticed that positive values of the charge Q significantly modify the GW waveform through lensing and the effect is present in the amplitude, as well as in the phase of the GW signal (Fig. 5). Thus, we expect that a BH lens without charge can be efficiently distinguished from a charged BH lens for $Q > 0$, while we expect such a distinction will be less efficient for $Q < 0$.

To get a better understanding of the prospective constraints on BH charge from future observations of microlensed GWs, we estimate the (approximate) Bayesian posteriors of Q from simulated observations of microlensed GWs. The GW signal microlensed by a BH can be parameterised by a set of source parameters $\vec{\theta}$ and lens parameters $\vec{\lambda}$. Their posterior distributions can be estimated from the observed data d using the Bayes theorem:

$$p(\vec{\theta}, \vec{\lambda}|d) = \frac{p(\vec{\theta}, \vec{\lambda})p(d|\vec{\theta}, \vec{\lambda}, \mathcal{H}_{\text{ML}})}{p(d|\mathcal{H}_{\text{ML}})}, \quad (17)$$

where $p(\vec{\theta}, \vec{\lambda})$ is the prior distribution of the source and lens parameters, $p(d|\vec{\theta}, \vec{\lambda}, \mathcal{H}_{\text{ML}})$ is the likelihood of getting data d given the parameters $\vec{\theta}, \vec{\lambda}$ and the hypothesis \mathcal{H}_{ML} that the data contains a microlensed GW signal. The denominator,

$p(d|\mathcal{H}_{\text{ML}})$, is the likelihood marginalised over all the parameters (called, the evidence of the hypothesis \mathcal{H}_{ML}).

The posterior $p(Q|d)$ of the charge can be computed by marginalising $p(\vec{\theta}, \vec{\lambda}|d)$ over all parameters except Q . For simplicity, we will assume that the lens parameters $\vec{\lambda}$ are largely uncorrelated with the source parameters $\vec{\theta}$. Hence we need to compute the likelihood only on $\vec{\lambda}$ for estimating prospective constraints on Q . This is a reasonable assumption although recent work has identified possible correlations between microlensing modulations and modulations induced by spin-induced precession [100]. An uncharged point mass lens in the background of a macro lens (e.g., a galaxy) could also introduce more complex modulations in the GW signal [55, 101–103], potentially mimicking some of the effect of a charged lens. Also, note that currently we assume non-spinning BH lenses. There could be some correlations between the charge and the spin of a BH (see, e.g., [87]). For the time being, we ignore these additional complexities.

It turns out that the lens parameters M_L, y are also largely uncorrelated with the charge Q (see, Fig. 6 for an illustration). Thus, to compute the expected bounds on Q , to a good approximation one needs to compute the likelihood in Q only. We employ the following approximation of the expectation value of the likelihood

$$\mathcal{L}(Q) \equiv \langle p(d|Q, \mathcal{H}_{\text{ML}}) \rangle \simeq \exp[-\rho^2 \mathcal{M}(Q_{\text{tr}}, Q)]. \quad (18)$$

Above ρ is the signal-to-noise ratio (SNR) of the signal in the data and $\mathcal{M}(Q_{\text{tr}}, Q)$ is the *mismatch* between the injected (true)

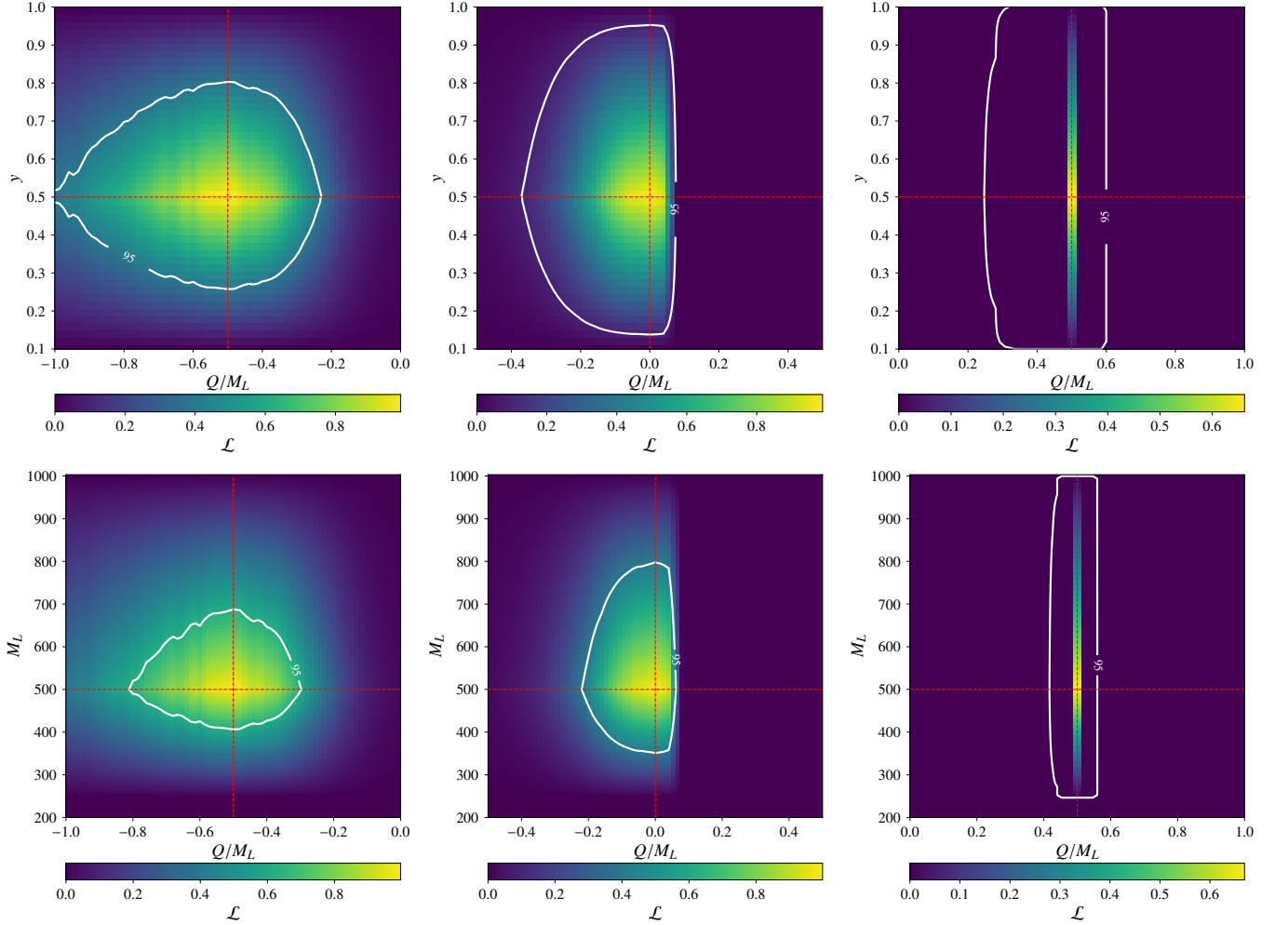


Figure 6. The top panel shows the 2D likelihood in the impact parameter y and charge Q/M_L computed from a GW signal with $\text{SNR} = 25$ microlensed by a charged BH of mass $M_L = 500M_\odot$. The true values of the impact parameter ($y = 0.5$) and charge ($Q/M_L = -0.5, 0, 0.5$) are indicated by the dashed red lines in each panel from left to right. The 95 percentile levels are indicated by white lines. The bottom panel shows the 2D likelihood in M_L and Q/M_L for a microlensed GW signal with $y = 0.5$. It can be seen that Q/M_L is largely uncorrelated with other parameters M_L and y .

waveform $h^L(f, Q_{\text{tr}})$ and the waveform $h^L(f, Q)$ with charge Q .

$$\mathcal{M}(Q_{\text{tr}}, Q) \equiv 1 - 4 \int_{f_{\text{low}}}^{f_{\text{upp}}} \frac{h^L(f, Q_{\text{tr}}) h^{L*}(f, Q) df}{S_n(f)}. \quad (19)$$

Here f_{low} and f_{upp} denote the lower and upper frequency cut-off of the detector band and $S_n(f)$ the one-sided power spectral density of the detector noise.

When we assume a flat prior in Q , the expectation value of the posterior distribution $P(Q|d)$ is the same as the likelihood $\mathcal{L}(Q)$. Hence we present $\mathcal{L}(Q)$ and its 90% credible upper limits in Fig. 7 and Fig. 8. In these figures, we have assumed the PSD of the advanced LIGO (aLIGO) detectors. Additionally, the unlensed signal is assumed to be due to a non-spinning equal mass BH binary with component masses $20M_\odot$ each. We compute the likelihood assuming true values of $(Q_{\text{tr}}/M_L) = 0, -0.1$ and -0.5 in Fig. 7 and true values of $(Q_{\text{tr}}/M_L) = 0, 0.1$ and 0.5 in Fig. 8.

It is evident from Eq.(18) that the likelihood drops when the mismatch between the true value Q_{tr} and the chosen value Q is large (i.e., when the two waveforms are very different) or when the SNR of the signal is large. These expected features can be seen in these figures. Negative values of Q are least constrained for smaller values of the impact parameter y and are slightly better constrained for larger impact parameter y (Fig. 7). Note that for smaller SNR and for smaller impact parameters, negative values of Q are unconstrained. Increasing the impact parameter, as well as for higher lens mass M_L , the constraints on Q significantly improve. Increasing the SNR further improves the situation.

On the other hand, and quite contrary to the negative Q case, as Fig. 8 demonstrates, even for SNR of 25, and impact parameter $y \sim 0.1$, positive values of Q can be measured with precision of $\Delta Q/Q \lesssim 0.1$ for larger lens masses. The situation improves drastically for higher SNR. For example, with an SNR of 100, values of $Q \gtrsim 0.02$ can be ruled out with ninety

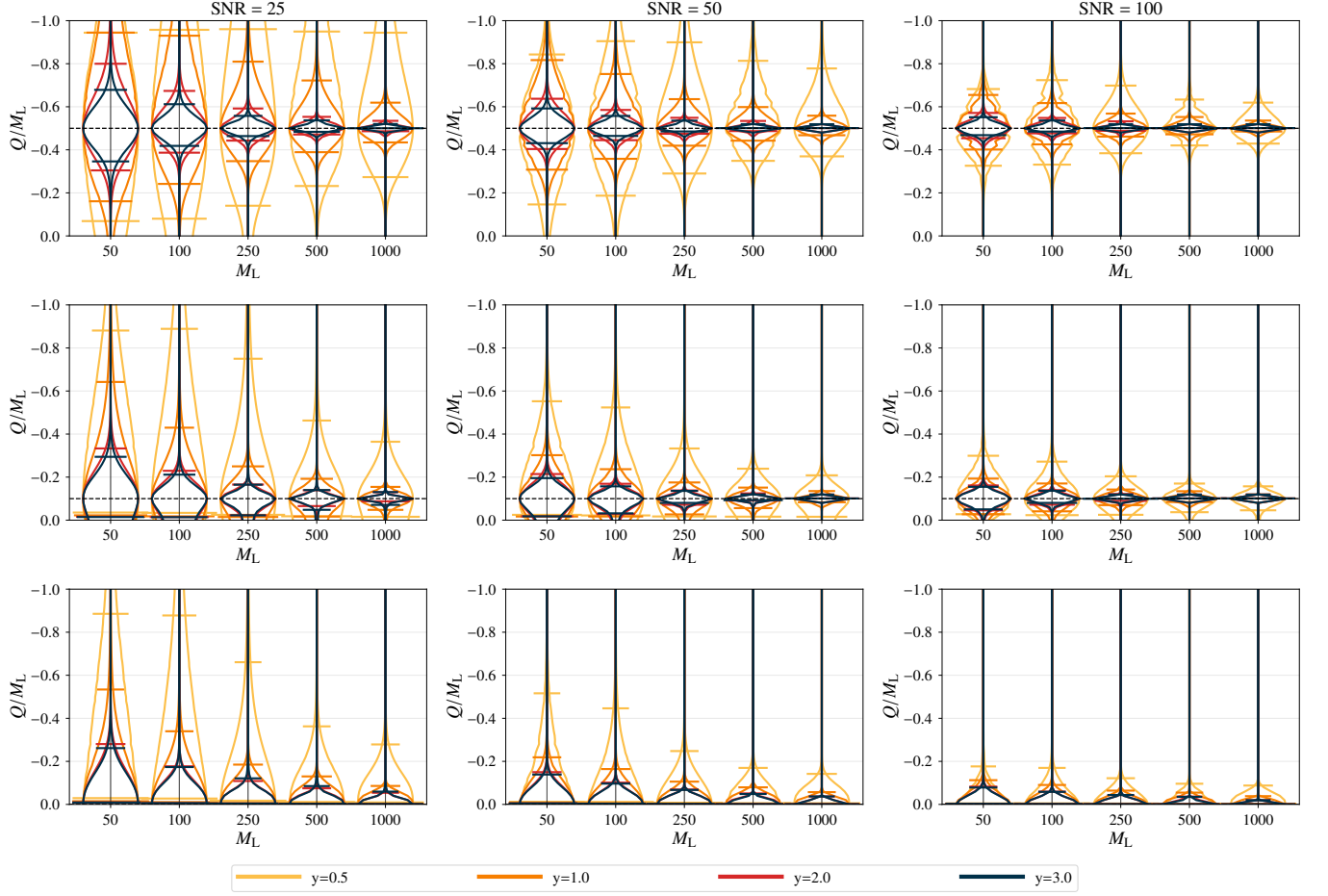


Figure 7. Likelihood plots with 90% credible bounds on Q/M_L using aLIGO PSD, for various values of impact parameter y (shown in the legend). Panels from left to right correspond to SNR values of 25, 50 and 100 respectively. In the top, middle and bottom panels, the GW signal is lensed by a BH of charge $Q_{tr}/M_L = -0.5, -0.1$ and 0 respectively (indicated by horizontal dashed black lines). Here, we use the prior $-1 \leq Q/M_L \leq 0$, that corresponds to situations such as the braneworld scenario.

percent confidence.

Thus using gravitational lensing of GWs, it is possible to rule out positive values of charge (of EM or modified gravity origin) with a percentage level accuracy. In contrast, for a negatively charged lens (expected in the presence of extra dimensions), the accuracy is at least an order weaker.

V. CONCLUSION

Upcoming observations are expected to detect gravitationally lensed GWs. One of the possible lenses is compact objects such as BHs. If the gravitational radii of these lenses are comparable to the wavelength of GWs, lensing will produce wave optics effects, producing characteristic deformations in the observed signals. The exact nature of these deformations will depend on the precise spacetime geometry (lensing potential) of the lens. Thus, lensing observations can potentially probe the detailed nature of these lensing objects.

In this paper, we derived an exact expression for the lensing potential of a ‘charged’ BH lens. The charge Q can have an EM

origin, in which case it is a positive definite quantity (Q is the square of the electric charge q), but can also arise in (at least) four different situations, all of which are beyond GR. These include — (a) the braneworld scenario, where the presence of an extra spatial dimension modifies Einstein’s equations, and introduces a charge term Q that is negative; (b) the Gauss-Bonnet theory in higher dimensions, which also leads to an effective four-dimensional spacetime with a negative charge; (c) $f(T)$ theories of gravity, as well as (d) a certain class of Horndeski theories also brings in a charge term in the spacetime metric, which is a positive quantity. Thus, negative values of the charge definitely hint at the presence of extra dimensions, while positive values of the charge can have an EM origin, or can also arise from modified theories of gravity. If one can detect the charge hair of a BH spacetime, it is possible to comment on the fundamental questions, e.g., the existence of extra dimension, as well as the signature of gravity theories beyond GR.

Using the lensing potential of charged BHs that we derived, we computed the deformation of the lensed GW signals considering wave optics effects. This was done using a numerical

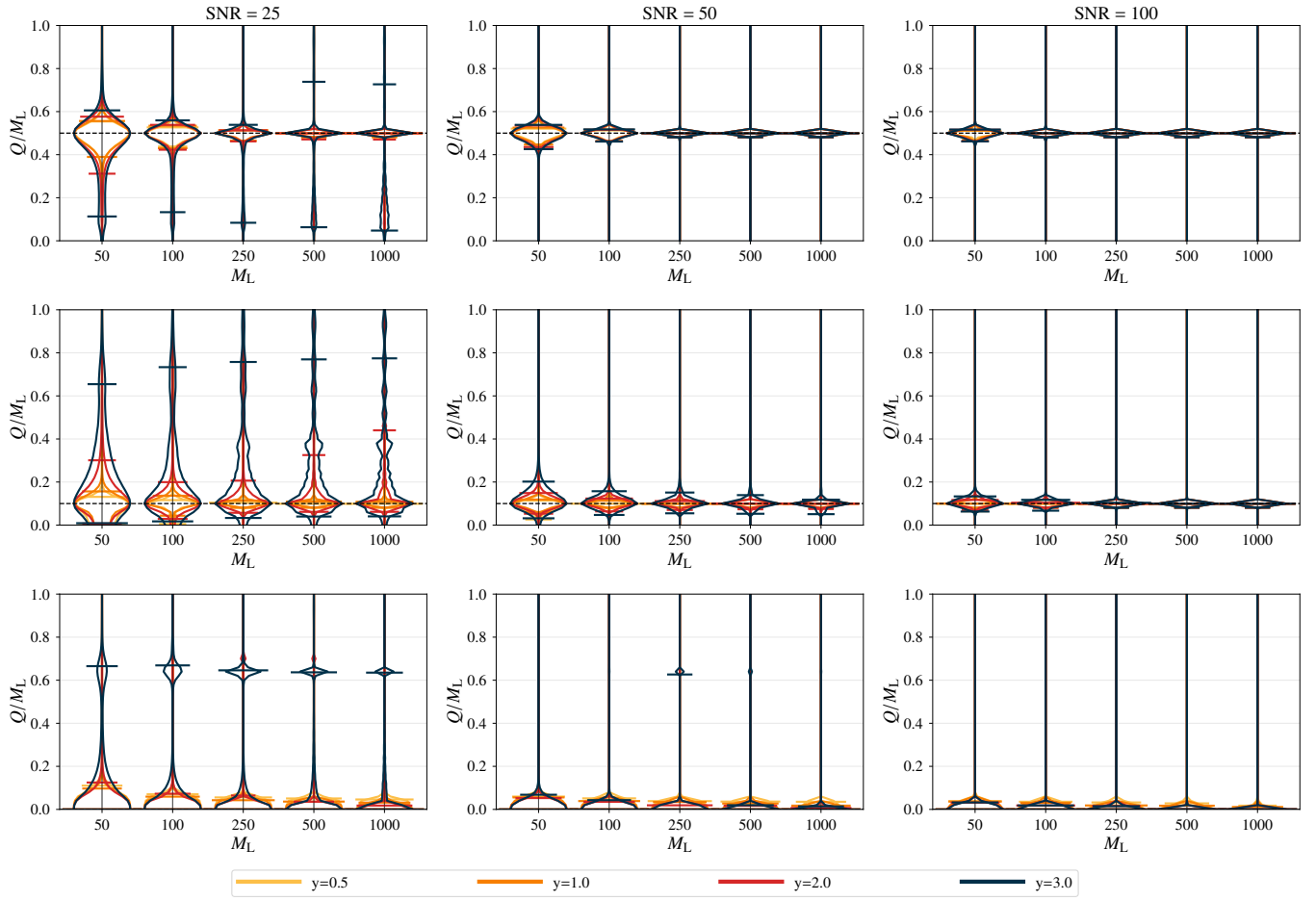


Figure 8. Same as Fig. 7, except that the GWs are lensed by BHs of charge $Q_{tr}/M_L = 0.5, 0.1$ and 0 respectively (indicated by horizontal dashed black lines). Here, we use the prior $0 \leq Q/M_L \leq 1$, which can correspond to a charge of EM or alternative gravity origin.

scheme that we recently developed. This scheme can be used to compute the frequency-dependent lensing magnification for arbitrary lensing potentials. We noticed interesting new observables in the case of charged lenses. Owing to the axial symmetry of the lensing potential, the images and the source always lie on a line on the lens plane (same as the case of uncharged lens). For a negatively charged lens there are always two images (same as the uncharged lens), while for a positively charged lens, there can be two or four images, depending on the value of the charge and the impact parameter. This new feature can be understood in terms of the (numerically computed) structure of the caustics of charged lenses. This introduces rich and complex effects in the lensed GW signals which are absent in those lensed by uncharged BHs. These additional features will help us to identify the presence of positively charged BH lenses, if they exist. On the other hand, negatively charged lenses produce features very similar to those of uncharged BHs, making it difficult to distinguish them from uncharged BHs.

We then explored the ability of future lensing observations to constrain the charge of the lens. We consider lensing observations by a single LIGO detector with sensitivity described by the PSD of the aLIGO observing run. We showed that the

charge can be constrained using observation of lensed GWs. In particular, positive values of the charge can be constrained to an accuracy of 10% (1%) if the lensed GW signal is detected with an SNR ~ 25 (100). On the other hand, negative values of the charge are constrained to a much lower precision, 15% at best (with SNR ~ 100). For smaller SNRs, practically all possible negative values of Q are allowed. In short, the presence of an extra dimension is much harder to detect using lensing of GWs, while there is excellent chance of detecting or constraining the presence of EM charge, or, theories beyond GR.

Note that the expected constraints that we present here employ an approximate likelihood, and neglect the possible correlations between the lensing-induced modulations in the GW signals and modulations induced by other physical effects such as orbital eccentricity of the binary source. We also ignored the possible degeneracy between a GW signal lensed by a charged BH and a GW signal lensed by an uncharged point mass lens in the presence of a macro lens (e.g., a galaxy), which can introduce more complex features. Additionally, we also neglected the effect of the spin of the BH lens. While we expect these broad conclusions to hold, the precise forecasts of the prospec-

tive constraints need to be revisited in the future considering these additional complexities.

The numerical scheme that we employ to compute lensing magnification for arbitrary lensing potentials is too expensive to employ in actual GW parameter estimation that will require a large number of likelihood evaluations. In order to employ in GW parameter estimation, we need to develop some surrogate/semi-analytical models that interpolate the numerically computed lensing magnifications over the parameter space of interest.

In this paper, we have worked with static and spherically symmetric spacetimes so far, and hence it would be interesting to generalize the same to rotating spacetimes, as all astrophysical objects are, in general, rotating. One could explore the possibility of measuring the spin of the compact object from lensing observations. One could also explore more general spacetimes: here we have considered the cases where $-g_{tt} = g^{rr}$; it will be useful to understand how to derive the lensing potential for spacetimes, with $-g_{tt} \neq g^{rr}$. Another possibility is probing the astrophysical environment of BHs using lensing observations. We hope to come back to these issues in future works.

Note that some of the modifications to GR that induce an effective charge on BHs could also cause other effects in the generation and propagation of GWs, which we neglect here. Our proposal should be seen as a way of effectively checking the consistency of the GW signal that is lensed by a BH in GR (in this paper the Schwarzschild metric). Any observed inconsistency with the Schwarzschild lens will need to be investigated further in order to ascertain the nature of the charge. This is similar in spirit to various other tests of GR using GW observations. In any case, future observations of lensed GWs are very likely to offer new ways of probing the nature of compact objects.

ACKNOWLEDGMENTS

We are grateful to Otto Hannuksela for the careful review of the manuscript and useful comments. We thank the members of the astrophysical relativity group at ICTS for their valuable input. We acknowledge the support of the Department of Atomic Energy, Government of India, under project no. RTI4001. M.A.S.'s research was, in addition, supported by the National Research Foundation of Korea under grant No. NRF-2021R1A2C2012473. S.C. thanks the Albert Einstein Institute for its warm hospitality, where a part of this work was performed. The visit to the Albert Einstein Institute is funded by the Max-Planck Society through its Max-Planck-India mobility grant. Computations were performed using the Alice computing cluster at the International Centre for Theoretical Sciences.

Appendix A: The lensing potential and its properties

In this appendix, we will provide the basic steps in deriving the lensing potential for a charged lens. For this purpose, we start by evaluating the two-dimensional Laplacian acting on $(\ln |\vec{x}|)^2$. Taking a double derivative with respect to x_1 yields,

$$\begin{aligned}\partial_{x_1}^2 (\ln |\vec{x}|)^2 &= \partial_{x_1} \left(2 \ln |\vec{x}| \frac{x_1}{|\vec{x}|^2} \right) \\ &= 2 \ln |\vec{x}| \frac{1}{|\vec{x}|^2} + 2 \frac{x_1^2}{|\vec{x}|^4} - 4 \ln |\vec{x}| \frac{x_1^2}{|\vec{x}|^4}.\end{aligned}\quad (\text{A1})$$

Along similar lines the derivative with respect to x_2 becomes,

$$\partial_{x_2}^2 (\ln |\vec{x}|)^2 = 2 \ln |\vec{x}| \frac{1}{|\vec{x}|^2} + 2 \frac{x_2^2}{|\vec{x}|^4} - 4 \ln |\vec{x}| \frac{x_2^2}{|\vec{x}|^4}.\quad (\text{A2})$$

Adding these two double derivatives, the two-dimensional Laplacian acting on $(\ln |\vec{x}|)^2$ gives us,

$$\begin{aligned}\nabla_x^2 (\ln |\vec{x}|)^2 &= \partial_{x_1}^2 (\ln |\vec{x}|)^2 + \partial_{x_2}^2 (\ln |\vec{x}|)^2 \\ &= 4 \ln |\vec{x}| \frac{1}{|\vec{x}|^2} + 2 \frac{x_1^2 + x_2^2}{|\vec{x}|^4} - 4 \ln |\vec{x}| \frac{x_1^2 + x_2^2}{|\vec{x}|^4} \\ &= \frac{2}{|\vec{x}|^2}.\end{aligned}\quad (\text{A3})$$

Thus the Laplacian acting on the $(\ln |\vec{x}|)^2$ indeed yields the energy density arising from the charged nature of the gravitational lens. This shows the origin of the expression for the lensing potential associated with the charged lens in the main text.

Let us now describe an interesting property of any axially symmetric lens system, namely the co-linear nature of the source and the images on the lens plane, which is also applicable in the present context. From the fact that the spacetime metric is axially symmetric, it follows that the lensing potential will also satisfy the same symmetry, i.e., $\psi(\vec{x}) = \psi(|\vec{x}|)$. The associated time delay is then given by,

$$\begin{aligned}t_d(\vec{x}, \vec{y}) &= \frac{|\vec{x} - \vec{y}|^2}{2} - \psi(|\vec{x}|) \\ &= \frac{|\vec{x}|^2}{2} - |\vec{x}||\vec{y}| \cos \theta + \frac{|\vec{y}|^2}{2} - \psi(|\vec{x}|),\end{aligned}\quad (\text{A4})$$

where $\vec{x} = (x_1, x_2) = (|\vec{x}| \cos \theta, |\vec{x}| \sin \theta)$, with θ being the angle between the vectors \vec{x} and \vec{y} . The location of the images can be found by solving $\nabla_x t_d(\vec{x}, \vec{y}) = 0$ as discussed in section II. This boils down to taking the derivative of the time delay function with respect to $|\vec{x}|$ and θ . Extremizing the time delay with respect to the angle θ yields,

$$\frac{\partial t_d}{\partial \theta} = |\vec{x}||\vec{y}| \sin \theta = 0,\quad (\text{A5})$$

which has only two solutions $\theta = 0, \pi$. This implies that the images will always lie along the direction of \vec{y} . In other words, for any axially symmetric lensing potential, the lens, the impact parameter, and the images are always co-linear on the lens plane. This feature can also be seen in Fig. 1.

-
- [1] R. Abbott *et al.* (LIGO Scientific, VIRGO, KAGRA), “GWTC-3: Compact Binary Coalescences Observed by LIGO and Virgo During the Second Part of the Third Observing Run,” (2021), [arXiv:2111.03606 \[gr-qc\]](#).
 - [2] B. P. Abbott *et al.* (LIGO Scientific, Virgo), “GW170817: Observation of Gravitational Waves from a Binary Neutron Star Inspiral,” *Phys. Rev. Lett.* **119**, 161101 (2017), [arXiv:1710.05832 \[gr-qc\]](#).
 - [3] B. P. Abbott *et al.* (LIGO Scientific, Virgo), “GW190425: Observation of a Compact Binary Coalescence with Total Mass $\sim 3.4M_{\odot}$,” *Astrophys. J. Lett.* **892**, L3 (2020), [arXiv:2001.01761 \[astro-ph.HE\]](#).
 - [4] R. Abbott *et al.* (LIGO Scientific, KAGRA, VIRGO), “Observation of Gravitational Waves from Two Neutron Star–Black Hole Coalescences,” *Astrophys. J. Lett.* **915**, L5 (2021), [arXiv:2106.15163 \[astro-ph.HE\]](#).
 - [5] R. Abbott *et al.* (LIGO Scientific, VIRGO, KAGRA), “Tests of General Relativity with GWTC-3,” (2021), [arXiv:2112.06861 \[gr-qc\]](#).
 - [6] LIGO Scientific, Virgo Collaborations, BP Abbott, R Abbott, TD Abbott, MR Abernathy, F Acernese, K Ackley, C Adams, T Adams, *et al.*, “Tests of general relativity with gw150914,” *Physical review letters* **116**, 221101 (2016).
 - [7] B. P. Abbott *et al.* (LIGO Scientific, Virgo), “Tests of General Relativity with the Binary Black Hole Signals from the LIGO–Virgo Catalog GWTC-1,” *Phys. Rev. D* **100**, 104036 (2019), [arXiv:1903.04467 \[gr-qc\]](#).
 - [8] R. Abbott *et al.* (LIGO Scientific, Virgo), “Properties and Astrophysical Implications of the $150 M_{\odot}$ Binary Black Hole Merger GW190521,” *Astrophys. J. Lett.* **900**, L13 (2020), [arXiv:2009.01190 \[astro-ph.HE\]](#).
 - [9] Abhirup Ghosh *et al.*, “Testing general relativity using golden black-hole binaries,” *Phys. Rev. D* **94**, 021101 (2016), [arXiv:1602.02453 \[gr-qc\]](#).
 - [10] Abhirup Ghosh, Nathan K. Johnson-Mcdaniel, Archisman Ghosh, Chandra Kant Mishra, Parameswaran Ajith, Walter Del Pozzo, Christopher P. L. Berry, Alex B. Nielsen, and Lionel London, “Testing general relativity using gravitational wave signals from the inspiral, merger and ringdown of binary black holes,” *Class. Quant. Grav.* **35**, 014002 (2018), [arXiv:1704.06784 \[gr-qc\]](#).
 - [11] B. P. Abbott *et al.* (LIGO Scientific, Virgo), “Tests of General Relativity with GW170817,” *Phys. Rev. Lett.* **123**, 011102 (2019), [arXiv:1811.00364 \[gr-qc\]](#).
 - [12] Clifford M Will, “Bounding the mass of the graviton using gravitational-wave observations of inspiralling compact binaries,” *Physical Review D* **57**, 2061 (1998).
 - [13] B. P. Abbott *et al.* (LIGO Scientific, Virgo), “GW170814: A Three-Detector Observation of Gravitational Waves from a Binary Black Hole Coalescence,” *Phys. Rev. Lett.* **119**, 141101 (2017), [arXiv:1709.09660 \[gr-qc\]](#).
 - [14] R. Abbott *et al.* (LIGO Scientific, Virgo), “Tests of general relativity with binary black holes from the second LIGO–Virgo gravitational-wave transient catalog,” *Phys. Rev. D* **103**, 122002 (2021), [arXiv:2010.14529 \[gr-qc\]](#).
 - [15] Hiroki Takeda, Soichiro Morisaki, and Atsushi Nishizawa, “Pure polarization test of GW170814 and GW170817 using waveforms consistent with modified theories of gravity,” *Phys. Rev. D* **103**, 064037 (2021), [arXiv:2010.14538 \[gr-qc\]](#).
 - [16] Isaac C. F. Wong, Peter T. H. Pang, Rico K. L. Lo, Tjonnie G. F. Li, and Chris Van Den Broeck, “Null-stream-based Bayesian Unmodeled Framework to Probe Generic Gravitational-wave Polarizations,” (2021), [arXiv:2105.09485 \[gr-qc\]](#).
 - [17] OA Hannuksela, K Haris, KKY Ng, S Kumar, AK Mehta, D Keitel, TGF Li, and P Ajith, “Search for gravitational lensing signatures in ligo-virgo binary black hole events,” *The Astrophysical Journal Letters* **874**, L2 (2019).
 - [18] Liang Dai, Barak Zackay, Tejaswi Venumadhav, Javier Roulet, and Matias Zaldarriaga, “Search for Lensed Gravitational Waves Including Morse Phase Information: An Intriguing Candidate in O2,” (2020), [arXiv:2007.12709 \[astro-ph.HE\]](#).
 - [19] Connor McIsaac, David Keitel, Thomas Collett, Ian Harry, Simone Mozzon, Oliver Edy, and David Bacon, “Search for strongly lensed counterpart images of binary black hole mergers in the first two ligo observing runs,” *Physical Review D* **102** (2020), 10.1103/physrevd.102.084031.
 - [20] R. Abbott *et al.* (LIGO Scientific, VIRGO), “Search for Lensing Signatures in the Gravitational-Wave Observations from the First Half of LIGO–Virgo’s Third Observing Run,” *Astrophys. J.* **923**, 14 (2021), [arXiv:2105.06384 \[gr-qc\]](#).
 - [21] R. Abbott *et al.* (LIGO Scientific, VIRGO, KAGRA), “Search for gravitational-lensing signatures in the full third observing run of the LIGO–Virgo network,” (2023), [arXiv:2304.08393 \[gr-qc\]](#).
 - [22] Justin Janquart *et al.*, “Follow-up Analyses to the O3 LIGO–Virgo–KAGRA Lensing Searches,” (2023), 10.1093/mnras/stad2909, [arXiv:2306.03827 \[gr-qc\]](#).
 - [23] Srashti Goyal, Shasvath Kapadia, Jean-Rene Cudell, Alvin K. Y. Li, and Juno C. L. Chan, “A rapid method for preliminary identification of subthreshold strongly lensed counterparts to superthreshold gravitational-wave events,” (2023), [arXiv:2306.04397 \[gr-qc\]](#).
 - [24] Tom Broadhurst, Jose M. Diego, and George Smoot, “Reinterpreting Low Frequency LIGO/Virgo Events as Magnified Stellar-Mass Black Holes at Cosmological Distances,” (2018), [arXiv:1802.05273 \[astro-ph.CO\]](#).
 - [25] T. Broadhurst, J. M. Diego, and G. F. Smoot, “A uniform stellar origin for binary black holes revealed by lensing,” (2022), [arXiv:2202.05861 \[astro-ph.GA\]](#).
 - [26] Srashti Goyal, K. Haris, Ajit Kumar Mehta, and Parameswaran Ajith, “Testing the nature of gravitational-wave polarizations using strongly lensed signals,” *Phys. Rev. D* **103**, 024038 (2021), [arXiv:2008.07060 \[gr-qc\]](#).
 - [27] Xi-Long Fan, Kai Liao, Marek Biesiada, Aleksandra Piórkowska-Kurpas, and Zong-Hong Zhu, “Speed of gravitational waves from strongly lensed gravitational waves and electromagnetic signals,” *Physical Review Letters* **118**, 091102 (2017).
 - [28] Ignacio Magaña Hernandez, “Measuring the polarization content of gravitational waves with strongly lensed binary black hole mergers,” (2022), [arXiv:2211.01272 \[gr-qc\]](#).
 - [29] Andreas Finke, Stefano Foffa, Francesco Iacovelli, Michele Maggiore, and Michele Mancarella, “Probing modified gravitational wave propagation with strongly lensed coalescing binaries,” *Physical Review D* **104** (2021), 10.1103/physrevd.104.084057.
 - [30] Harsh Narola, Justin Janquart, Leila Haegel, K. Haris, Otto A. Hannuksela, and Chris Van Den Broeck, “How well can modified gravitational wave propagation be constrained with strong lensing?” (2023), [arXiv:2308.01709 \[gr-qc\]](#).
 - [31] Adrian Ka-Wai Chung and Tjonnie G. F. Li, “Lensing of gravitational waves as a novel probe of graviton mass,” *Physical*

- Review D **104** (2021), [10.1103/physrevd.104.124060](#).
- [32] Srashiti Goyal, Aditya Vijaykumar, Jose María Ezquiaga, and Miguel Zumalacárregui, “Probing lens-induced gravitational-wave birefringence as a test of general relativity,” *Physical Review D* **108** (2023), [10.1103/physrevd.108.024052](#).
- [33] Suvodip Mukherjee, Benjamin D Wandelt, and Joseph Silk, “Probing the theory of gravity with gravitational lensing of gravitational waves and galaxy surveys,” *Monthly Notices of the Royal Astronomical Society* **494**, 1956–1970 (2020).
- [34] Thomas E. Collett and David Bacon, “Testing the speed of gravitational waves over cosmological distances with strong gravitational lensing,” *Physical Review Letters* **118** (2017), [10.1103/physrevlett.118.091101](#).
- [35] Soumyadip Basak, Aditya Kumar Sharma, Shasvath J. Kapadia, and Parameswaran Ajith, “Prospects for the Observation of Continuous Gravitational Waves from Spinning Neutron Stars Lensed by the Galactic Supermassive Black Hole,” *Astrophys. J. Lett.* **942**, L31 (2023), [arXiv:2205.00022 \[gr-qc\]](#).
- [36] Mukesh Kumar Singh, Shasvath J. Kapadia, Soumyadip Basak, Parameswaran Ajith, and Shriharsh P. Tendulkar, “Déjà-vu et Déjà-entendu: Associating fast radio bursts with compact binary mergers via gravitational lensing,” (2023), [arXiv:2304.02879 \[astro-ph.HE\]](#).
- [37] Sourabh Magare, Shasvath J. Kapadia, Anupreeta More, Mukesh Kumar Singh, Parameswaran Ajith, and A. N. Ramprakash, “Gear-up for the Action Replay: Leveraging Lensing for Enhanced Gravitational-Wave Early-Warning,” (2023), [arXiv:2302.02916 \[astro-ph.HE\]](#).
- [38] S. Basak, A. Ganguly, K. Haris, S. Kapadia, A. K. Mehta, and P. Ajith, “Constraints on Compact Dark Matter from Gravitational Wave Microlensing,” *Astrophys. J.* **926**, L28 (2022), [arXiv:2109.06456 \[gr-qc\]](#).
- [39] Souvik Jana, Shasvath J. Kapadia, Tejaswi Venumadhav, and Parameswaran Ajith, “Cosmography using strongly lensed gravitational waves from binary black holes,” (2022), [arXiv:2211.12212 \[astro-ph.CO\]](#).
- [40] Otto A Hannuksela, Thomas E Collett, Mesut Çalışkan, and Tjonnie GF Li, “Localizing merging black holes with sub-arcsecond precision using gravitational-wave lensing,” *Monthly Notices of the Royal Astronomical Society* **498**, 3395–3402 (2020).
- [41] Hans C Ohanian, “On the focusing of gravitational radiation,” *International Journal of Theoretical Physics* **9**, 425–437 (1974).
- [42] S. Deguchi and W. D. Watson, “Diffraction in Gravitational Lensing for Compact Objects of Low Mass,” *Astrophys. J.* **307**, 30 (1986).
- [43] Yun Wang, Albert Stebbins, and Edwin L. Turner, “Gravitational lensing of gravitational waves from merging neutron star binaries,” *Phys. Rev. Lett.* **77**, 2875–2878 (1996).
- [44] Takahiro T. Nakamura, “Gravitational lensing of gravitational waves from inspiraling binaries by a point mass lens,” *Phys. Rev. Lett.* **80**, 1138–1141 (1998).
- [45] Matthias Bartelmann, “Gravitational lensing,” *Classical and Quantum Gravity* **27**, 233001 (2010).
- [46] Ken K. Y. Ng, Kaze W. K. Wong, Tom Broadhurst, and Tjonnie G. F. Li, “Precise LIGO Lensing Rate Predictions for Binary Black Holes,” *Phys. Rev. D* **97**, 023012 (2018), [arXiv:1703.06319 \[astro-ph.CO\]](#).
- [47] Liang Dai, Tejaswi Venumadhav, and Kris Sigurdson, “Effect of lensing magnification on the apparent distribution of black hole mergers,” *Phys. Rev. D* **95**, 044011 (2017), [arXiv:1605.09398 \[astro-ph.CO\]](#).
- [48] Graham P. Smith, Mathilde Jauzac, John Veitch, Will M. Farr, Richard Massey, and Johan Richard, “What if LIGO’s gravitational wave detections are strongly lensed by massive galaxy clusters?” *Mon. Not. Roy. Astron. Soc.* **475**, 3823–3828 (2018), [arXiv:1707.03412 \[astro-ph.HE\]](#).
- [49] Robert Kormann, Peter Schneider, and Matthias Bartelmann, “Isothermal elliptical gravitational lens models,” *Astronomy and Astrophysics* **284**, 285–299 (1994).
- [50] LVE Koopmans, A Bolton, T Treu, O Czoske, MW Auger, M Barnabe, S Vegetti, R Gavazzi, LA Moustakas, and S Burles, “The structure and dynamics of massive early-type galaxies: On homology, isothermality, and isotropy inside one effective radius,” *The Astrophysical Journal* **703**, L51 (2009).
- [51] K. Haris, Ajit Kumar Mehta, Sumit Kumar, Tejaswi Venumadhav, and Parameswaran Ajith, “Identifying strongly lensed gravitational wave signals from binary black hole mergers,” (2018), [arXiv:1807.07062 \[gr-qc\]](#).
- [52] Anupreeta More and Surhud More, “Improved statistic to identify strongly lensed gravitational wave events,” *Mon. Not. Roy. Astron. Soc.* **515**, 1044–1051 (2022), [arXiv:2111.03091 \[astro-ph.CO\]](#).
- [53] Ryuichi Takahashi and Takashi Nakamura, “Wave effects in the gravitational lensing of gravitational waves from chirping binaries,” *The Astrophysical Journal* **595**, 1039 (2003).
- [54] Sunghoon Jung and Chang Sub Shin, “Gravitational-Wave Fringes at LIGO: Detecting Compact Dark Matter by Gravitational Lensing,” *Phys. Rev. Lett.* **122**, 041103 (2019), [arXiv:1712.01396 \[astro-ph.CO\]](#).
- [55] J. M. Diego, O. A. Hannuksela, P. L. Kelly, T. Broadhurst, K. Kim, T. G. F. Li, G. F. Smoot, and G. Pagano, “Observational signatures of microlensing in gravitational waves at LIGO/Virgo frequencies,” *Astron. Astrophys.* **627**, A130 (2019), [arXiv:1903.04513 \[astro-ph.CO\]](#).
- [56] Juan Urrutia and Ville Vaskonen, “Lensing of gravitational waves as a probe of compact dark matter,” *Monthly Notices of the Royal Astronomical Society* **509**, 1358–1365 (2022).
- [57] Takahiro T. Nakamura and Shuji Deguchi, “Wave optics in gravitational lensing,” *Progress of Theoretical Physics Supplement* **133**, 137–153 (1999).
- [58] Justin C. Feng, Sumanta Chakraborty, and Vitor Cardoso, “Shielding a charged black hole,” *Phys. Rev. D* **107**, 044050 (2023), [arXiv:2211.05261 \[gr-qc\]](#).
- [59] D. Marín Pina, M. Orselli, and D. Pica, “Event horizon of a charged black hole binary merger,” *Phys. Rev. D* **106**, 084012 (2022), [arXiv:2204.08841 \[gr-qc\]](#).
- [60] Gabriele Bozzola and Vasileios Paschalidis, “General Relativistic Simulations of the Quasicircular Inspiral and Merger of Charged Black Holes: GW150914 and Fundamental Physics Implications,” *Phys. Rev. Lett.* **126**, 041103 (2021), [arXiv:2006.15764 \[gr-qc\]](#).
- [61] D. M. Eardley and W. H. Press, “Astrophysical processes near black holes,” *Ann. Rev. Astron. Astrophys.* **13**, 381–422 (1975).
- [62] Tetsuya Shiromizu, Kei-ichi Maeda, and Misao Sasaki, “The Einstein equation on the 3-brane world,” *Phys. Rev. D* **62**, 024012 (2000), [arXiv:gr-qc/9910076](#).
- [63] Naresh Dadhich, Roy Maartens, Philippos Papadopoulos, and Vahid Rezanian, “Black holes on the brane,” *Phys. Lett. B* **487**, 1–6 (2000), [arXiv:hep-th/0003061](#).
- [64] T. Harko and M. K. Mak, “Vacuum solutions of the gravitational field equations in the brane world model,” *Phys. Rev. D* **69**, 064020 (2004), [arXiv:gr-qc/0401049](#).
- [65] A. N. Aliev and A. E. Gumrukcuoglu, “Charged rotating black holes on a 3-brane,” *Phys. Rev. D* **71**, 104027 (2005), [arXiv:hep-th/0502223](#).
- [66] Hideki Maeda and Naresh Dadhich, “Matter without matter: Novel Kaluza-Klein spacetime in Einstein-Gauss-Bonnet grav-

- ity,” *Phys. Rev. D* **75**, 044007 (2007), [arXiv:hep-th/0611188](#).
- [67] Eugeny Babichev, Christos Charmousis, and Mokhtar Hossaine, “Charged Galileon black holes,” *JCAP* **05**, 031 (2015), [arXiv:1503.02545 \[gr-qc\]](#).
- [68] José Barrientos, Fabrizio Cordonier-Tello, Fernando Izaurieta, Perla Medina, Daniela Narbona, Eduardo Rodríguez, and Omar Valdivia, “Nonminimal couplings, gravitational waves, and torsion in Horndeski’s theory,” *Phys. Rev. D* **96**, 084023 (2017), [arXiv:1703.09686 \[gr-qc\]](#).
- [69] Eugeny Babichev and Christos Charmousis, “Dressing a black hole with a time-dependent Galileon,” *JHEP* **08**, 106 (2014), [arXiv:1312.3204 \[gr-qc\]](#).
- [70] Lorenzo Iorio and Emmanuel N. Saridakis, “Solar system constraints on $f(T)$ gravity,” *Mon. Not. Roy. Astron. Soc.* **427**, 1555 (2012), [arXiv:1203.5781 \[gr-qc\]](#).
- [71] Salvatore Capozziello, P. A. Gonzalez, Emmanuel N. Saridakis, and Yerko Vasquez, “Exact charged black-hole solutions in D-dimensional $f(T)$ gravity: torsion vs curvature analysis,” *JHEP* **02**, 039 (2013), [arXiv:1210.1098 \[hep-th\]](#).
- [72] Sumanta Chakraborty and Soumitra SenGupta, “Solar system constraints on alternative gravity theories,” *Phys. Rev. D* **89**, 026003 (2014), [arXiv:1208.1433 \[gr-qc\]](#).
- [73] Sourav Bhattacharya and Sumanta Chakraborty, “Constraining some Horndeski gravity theories,” *Phys. Rev. D* **95**, 044037 (2017), [arXiv:1607.03693 \[gr-qc\]](#).
- [74] Sajal Mukherjee and Sumanta Chakraborty, “Horndeski theories confront the Gravity Probe B experiment,” *Phys. Rev. D* **97**, 124007 (2018), [arXiv:1712.00562 \[gr-qc\]](#).
- [75] Andrea Maselli, Leonardo Gualtieri, Paolo Pani, Luigi Stella, and Valeria Ferrari, “Testing Gravity with Quasi Periodic Oscillations from accreting Black Holes: the Case of the Einstein-Dilaton-Gauss-Bonnet Theory,” *Astrophys. J.* **801**, 115 (2015), [arXiv:1412.3473 \[astro-ph.HE\]](#).
- [76] Zdeněk Stuchlík and Andrea Kotrllová, “Orbital resonances in discs around braneworld Kerr black holes,” *Gen. Rel. Grav.* **41**, 1305–1343 (2009), [arXiv:0812.5066 \[astro-ph\]](#).
- [77] Indrani Banerjee, Sumanta Chakraborty, and Soumitra SenGupta, “Looking for extra dimensions in the observed quasi-periodic oscillations of black holes,” *JCAP* **09**, 037 (2021), [arXiv:2105.06636 \[gr-qc\]](#).
- [78] Indrani Banerjee, Sumanta Chakraborty, and Soumitra SenGupta, “Excavating black hole continuum spectrum: Possible signatures of scalar hairs and of higher dimensions,” *Phys. Rev. D* **96**, 084035 (2017), [arXiv:1707.04494 \[gr-qc\]](#).
- [79] Enrico Barausse and Kent Yagi, “Gravitation-Wave Emission in Shift-Symmetric Horndeski Theories,” *Phys. Rev. Lett.* **115**, 211105 (2015), [arXiv:1509.04539 \[gr-qc\]](#).
- [80] Bobir Toshmatov, Zdeněk Stuchlík, Jan Schee, and Bobomurat Ahmedov, “Quasinormal frequencies of black hole in the braneworld,” *Phys. Rev. D* **93**, 124017 (2016), [arXiv:1605.02058 \[gr-qc\]](#).
- [81] David Andriot and Gustavo Lucena Gómez, “Signatures of extra dimensions in gravitational waves,” *JCAP* **06**, 048 (2017), [Erratum: *JCAP* **05**, E01 (2019)], [arXiv:1704.07392 \[hep-th\]](#).
- [82] Sumanta Chakraborty, Kabir Chakravarti, Sukanta Bose, and Soumitra SenGupta, “Signatures of extra dimensions in gravitational waves from black hole quasinormal modes,” *Phys. Rev. D* **97**, 104053 (2018), [arXiv:1710.05188 \[gr-qc\]](#).
- [83] Kabir Chakravarti, Sumanta Chakraborty, Khun Sang Phukon, Sukanta Bose, and Soumitra SenGupta, “Constraining extra-spatial dimensions with observations of GW170817,” *Class. Quant. Grav.* **37**, 105004 (2020), [arXiv:1903.10159 \[gr-qc\]](#).
- [84] Akash K. Mishra, Abhirup Ghosh, and Sumanta Chakraborty, “Constraining extra dimensions using observations of black hole quasi-normal modes,” *Eur. Phys. J. C* **82**, 820 (2022), [arXiv:2106.05558 \[gr-qc\]](#).
- [85] Akash K. Mishra, Gregorio Carullo, and Sumanta Chakraborty, “Bounds on tidal charges from gravitational-wave ringdown observations,” (2023), [arXiv:2311.03556 \[gr-qc\]](#).
- [86] Pawan Kumar Gupta, Thomas F. M. Spieksma, Peter T. H. Pang, Gideon Koekoek, and Chris Van Den Broeck, “Bounding dark charges on binary black holes using gravitational waves,” *Physical Review D* **104** (2021), 10.1103/physrevd.104.063041.
- [87] Gregorio Carullo, Danny Laghi, Nathan K. Johnson-McDaniel, Walter Del Pozzo, Oscar J. C. Dias, Mahdi Godazgar, and Jorge E. Santos, “Constraints on Kerr-Newman black holes from merger-ringdown gravitational-wave observations,” *Phys. Rev. D* **105**, 062009 (2022), [arXiv:2109.13961 \[gr-qc\]](#).
- [88] Hua-Peng Gu, Hai-Tian Wang, and Lijing Shao, “Constraints on charged black holes from merger-ringdown signals in gwtc-3 and prospects for the einstein telescope,” (2023), [arXiv:2310.10447 \[gr-qc\]](#).
- [89] Sumanta Chakraborty and Soumitra SenGupta, “Strong gravitational lensing — A probe for extra dimensions and Kalb-Ramond field,” *JCAP* **07**, 045 (2017), [arXiv:1611.06936 \[gr-qc\]](#).
- [90] Indrani Banerjee, Sumanta Chakraborty, and Soumitra SenGupta, “Hunting extra dimensions in the shadow of Sgr A*,” *Phys. Rev. D* **106**, 084051 (2022), [arXiv:2207.09003 \[gr-qc\]](#).
- [91] Sunny Vagnozzi *et al.*, “Horizon-scale tests of gravity theories and fundamental physics from the Event Horizon Telescope image of Sagittarius A,” *Class. Quant. Grav.* **40**, 165007 (2023), [arXiv:2205.07787 \[gr-qc\]](#).
- [92] Indrani Banerjee, Sumanta Chakraborty, and Soumitra SenGupta, “Silhouette of M87*: A New Window to Peek into the World of Hidden Dimensions,” *Phys. Rev. D* **101**, 041301 (2020), [arXiv:1909.09385 \[gr-qc\]](#).
- [93] T. Padmanabhan, *Gravitation: Foundations and Frontiers* (Cambridge University Press, Cambridge, UK, 2010).
- [94] S. H. Hendi, “Charged BTZ-like Black Holes in Higher Dimensions,” *Eur. Phys. J. C* **71**, 1551 (2011), [arXiv:1007.2704 \[gr-qc\]](#).
- [95] S. H. Hendi, A. M. Tavakkoli, S. Panahiyan, B. Eslam Panah, and E. Hackmann, “Simulation of geodesic trajectory of charged BTZ black holes in massive gravity,” *Eur. Phys. J. C* **80**, 524 (2020), [arXiv:2002.01302 \[gr-qc\]](#).
- [96] Zi-Yu Tang, Cheng-Yong Zhang, Mahdi Kord Zangeneh, Bin Wang, and Joel Saavedra, “Thermodynamical and dynamical properties of Charged BTZ Black Holes,” *Eur. Phys. J. C* **77**, 390 (2017), [arXiv:1610.01744 \[hep-th\]](#).
- [97] Chiranjeeb Singha, Sumanta Chakraborty, and Naresh Dadhich, “Strong cosmic censorship conjecture for a charged BTZ black hole,” *JHEP* **06**, 028 (2022), [arXiv:2203.07708 \[gr-qc\]](#).
- [98] Roger Blandford and Ramesh Narayan, “Fermat’s Principle, Caustics, and the Classification of Gravitational Lens Images,” *Astrophys. J.* **310**, 568 (1986).
- [99] Andrew Ulmer and Jeremy Goodman, “Femtolensing: Beyond the semiclassical approximation,” *The Astrophysical Journal* **442**, 67 (1995).
- [100] Anuj Mishra, Ashish Kumar Meena, Anupreeta More, and Sukanta Bose, “Exploring the Impact of Microlensing on Gravitational Wave Signals: Biases, Population Characteristics, and Prospects for Detection,” (2023), [arXiv:2306.11479 \[astro-ph.CO\]](#).
- [101] Ashish Kumar Meena and J. S. Bagla, “Gravitational lensing of gravitational waves: wave nature and prospects for detection,” *Mon. Not. Roy. Astron. Soc.* **492**, 1127–1134 (2020), [arXiv:1903.11809 \[astro-ph.CO\]](#).

- [102] Mark H. Y. Cheung, Joseph Gais, Otto A. Hannuksela, and Tjonnie G. F. Li, “Stellar-mass microlensing of gravitational waves,” *Mon. Not. Roy. Astron. Soc.* **503**, 3326–3336 (2021), [arXiv:2012.07800 \[astro-ph.HE\]](#).
- [103] Anuj Mishra, Ashish Kumar Meena, Anupreeta More, Sukanta Bose, and Jasjeet Singh Bagla, “Gravitational lensing of gravitational waves: effect of microlens population in lensing galaxies,” *Mon. Not. Roy. Astron. Soc.* **508**, 4869–4886 (2021), [arXiv:2102.03946 \[astro-ph.CO\]](#).